Energy 324 (2025) 136037

Contents lists available at ScienceDirect

Energy

journal homepage: www.elsevier.com/locate/energy

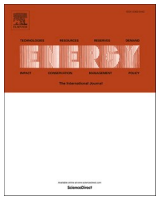

Importance of pore and chemical structures of activated biochar on bio-oil deoxygenation during online catalytic cracking of volatiles over activated biochars obtained from different activation methods

Derui Yang [a,b], Wojciech Jerzak [c], Yusuf Makarfi Isa [d], Xing Xie [a], Dan Lin [a], Haiping Yang [e], Shihong Zhang [e], Youjian Zhu [f,**], Bin Li [a,b,*]

[a] School of Energy and Power Engineering, Jiangsu University, Zhenjiang, 212013, China
[b] School of Engineering, Anhui Agricultural University, Hefei, 230036, China
[c] Faculty of Metals Engineering and Industrial Computer Science, AGH University of Krakow, Mickiewicza Av. 30, 30-059, Krakow, Poland
[d] School of Chemical and Metallurgical Engineering, University of the Witwatersrand, Johannesburg, 2050, South Africa
[e] State Key Laboratory of Coal Combustion, School of Energy and Power Engineering, Huazhong University of Science and Technology, Wuhan, 430074, China
[f] College of New Energy, Zhengzhou University of Light Industry, Zhengzhou, 450001, China

ARTICLE INFO

Keywords:
Bio-oil
Catalytic cracking
Activated biochar
Activation methods
Pore structure

ABSTRACT

Activated biochar (ABC) is a promising catalyst for bio-oil deoxygenation, its catalytic performance is closely related to the physicochemical structures. In this study, the online catalytic cracking of pine sawdust volatiles over ABCs obtained from different activation methods was conducted in a fixed-bed reactor at 500 °C. ABC participated in reactions with reduced O-containing surface groups and porosity. The ultra-micropores (<0.68 nm) in biochar were fully blocked by coke, an appropriate micropore and mesopore distribution (e.g., 1–3 nm) was preferable for retaining its catalytic activity. Bio-oil was deoxygenated over char surface in the form of CO (predominately), CO_2 and H_2O, along with dehydrogenation and dealkylation reactions. The O-containing surface groups of ABCs acted as active sites, but their porous structures played a dominated role during bio-oil deoxygenation, the depth/degree of bio-oil cracking/deoxygenation was determined by the BET surface areas obtained from different activation methods. KOH-ABC and K_2CO_3-ABC with high porosities deeply deoxygenated bio-oil to selectively form phenols and aromatics. H_2O-ABC with medium BET surface area showed moderate deoxygenation ability, resulting in more carbonyls formation. In contrast, $ZnCl_2$-ABC, H_3PO_4-ABC, $KMnO_4$-ABC, and CO_2-ABC with less porosities exhibited low cracking/deoxygenation abilities. This study provides insight into optimizing biochar activation strategies for bio-oil catalytic deoxygenation.

1. Introduction

Biomass, as the only renewable carbon source in nature, is widely recognized as one of the most promising solutions to global demands on carbon-based materials, chemicals, and fuels due to its abundance and the ability to recycle carbon within natural cycles. Pyrolysis of biomass, as a thermochemical conversion process, involves the decomposition of biomass in the absence or presence of limited O_2, yielding bio-oil, biochar, and non-condensable gases [1]. However, bio-oil obtained through direct pyrolysis has several drawbacks, such as high O content (35–50 wt %), low calorific value (14–19 MJ/kg), and strong corrosion (pH value of 2–3), which limit its direct utilization [2]. Therefore, catalytic upgrading is essential to improve bio-oil quality by reducing its O content and enhancing its chemical stability.

Among various catalysts, biochar has emerged as a potential candidate for bio-oil deoxygenation. In our previous studies, it was found that the O-containing functional groups and aromatic carbon skeletons on the biochar surface could act as active sites for O removal from volatiles or bio-oil, primarily in the form of CO and CO_2 [3–5]. Hu et al. [6] found that the presence of biochar promoted the conversion of tar into non-condensable gases, the contents of ketones, esters, phenols, and furans in liquid products increased while the content of aromatic compounds decreased. Biochar can be obtained from various cheap and easily obtainable feedstocks, including terrestrial biomass [7] and algae

* Corresponding author. School of Energy and Power Engineering, Jiangsu University, Zhenjiang 212013, China.
** Corresponding author.
E-mail addresses: yjzhu01@hotmail.com (Y. Zhu), libin198520@126.com (B. Li).

https://doi.org/10.1016/j.energy.2025.136037
Received 5 December 2024; Received in revised form 21 March 2025; Accepted 5 April 2025
Available online 7 April 2025

[8]. Compared to other catalysts, such as molecular sieve and noble metal catalysts, biochar offers advantages such as simple preparation, cost-effectiveness, and the possibility of energy recovery through combustion or gasification after deactivation [9]. The catalytic activity of biochar is highly related to its pore structure [10] and active surface functional groups [11]. However, biochar derived from direct pyrolysis typically exhibits limited porosity [12] and poor surface functionality, necessitating further modification.

Activation of biochar is a crucial method for enhancing the pore structure and surface chemistry, thereby improving its catalytic performance for bio-oil upgrading [13,14]. For instance, Liu et al. [10] reported that biochar activated with CO_2 increased the phenol content of bio-oil to 78.12 % at 400 °C and it further increased to 97 % at 600 °C during pine sawdust pyrolysis. Similarly, Zhang et al. [15] demonstrated that phosphoric acid-activated cornstalk biochar achieved 96.7 % selectivity for phenolic compounds along with high CO production (42.1 %) during cellulose pyrolysis. In another study, KOH-activated brown algae biochar facilitated the dehydration, decarboxylation, and decarbonylation of pyrolysis intermediates, yielding a maximum monophenol content of 48.99 % in bio-oil [16].

The activation of biochar involves etching of its surface by probe molecules. Depending on the type of activator used, activation can be categorized into physical and chemical methods [17]. Physical activation typically utilizes CO_2 or steam (H_2O), which react with biochar at elevated temperatures [18]. While chemical activation involves high-temperature reactions with chemical reagents such as KOH, K_2CO_3, $ZnCl_2$, and H_3PO_4 [19,20]. Studies have shown that different activation methods result in significant variations in the physicochemical properties of biochar, including its porosity and surface chemical structure [21–23]. These differences suggest that the catalytic performance of biochar in the upgrading of bio-oil will vary depending on the activation method used [12]. However, a systematic investigation of the catalytic cracking performance of activated biochar synthesized through different methods is still lacking. How different activation strategies influencing the physicochemical properties of biochar and the underlying mechanisms in the catalytic cracking process are essential. In particular, the importance of pore and surface chemical structures of biochar obtained from different activation methods still needs to be further evaluated. Such research will provide valuable insights for optimizing activation strategies in terms of bio-oil deoxygenation and expanding the practical application of biochar in bio-oil upgrading.

Therefore, this study would comprehensively investigate the effects of different activation methods on the physicochemical properties of biochar, including both physical and chemical activations, and the catalytic performance of various activated biochars was evaluated through online catalytic cracking of biomass pyrolysis volatiles in a fixed-bed reactor. Various characterization techniques were applied to analyze the physicochemical properties of the activated biochar before and after the reaction, as well as the gas and liquid products generated during pyrolysis. The primary factors influencing the catalytic performance of activated biochar were identified, along with the structural evolution of the biochar during the reaction. Additionally, the possible mechanism of catalytic bio-oil cracking was explored. The results in this study could provide valuable insights and experimental data to support its employment in practical applications.

2. Experimental

2.1. Raw materials

Acid-washed pine sawdust was selected as the biomass feedstock to generate volatiles for online catalytic cracking as well as to synthesize activated biochar. Alkali and alkaline earth metal species (AAEMs) in pine sawdust were removed by acid washing to eliminate their influence on the pyrolysis and catalytic cracking processes. The acid-washing process was as follows: approximately 60 g of pine sawdust was weighed and immersed in 1 L of a 1 wt% HCl solution, it was stirred at room temperature for 2 h and stood for 24 h. The solution was then filtered, and the pine sawdust was thoroughly rinsed with deionized water until the pH became neutral. The acid-washed pine sawdust was then dried at 105 °C for 24 h and stored in a sealed desiccator prior to future use.

The chemical activators of KOH, K_2CO_3, $ZnCl_2$, H_3PO_4, and $KMnO_4$, were purchased from Sinopharm Chemical Reagent Co., Ltd with analytical purities. High-purity of CO_2 with 99.999 % purity from a local gas supplier as well as steam (H_2O) were used as the physical activators. Concentrated hydrochloric acid with analytical purity (36–38 wt%) from Sinopharm Chemical Reagent Co., Ltd was diluted to 1 wt% HCl solution using for acid washing. The deionized (DI) water was also applied for the washing process.

2.2. Preparation of activated biochar

Activated biochar was prepared using a two-step process. Firstly, biochar was produced by pyrolyzing acid-washed sawdust in a tube furnace at 600 °C for 30 min under a N_2 flow of 500 mL/min. After pyrolysis, the biochar was quickly removed from the heating zone and cooled to room temperature under an N_2 atmosphere. It was collected in a sample bottle with a closed cap and stored in a desiccator for further use. The second step involved activating the biochar using both physical and chemical activators. For chemical activation, 3 g of the above made biochar was evenly dry-mixed with 9 g of activator (e.g., KOH, K_2CO_3, $ZnCl_2$, H_3PO_4, or $KMnO_4$). The mixture was activated in a tube furnace at 800 °C for 2 h under N_2 at 500 mL/min. After activation, the cooled solid sample was immersed in a 1 wt% HCl solution, stirred for 2 h, stood for 24 h, and then rinsed with deionized water until neutral. The obtained activated biochar was finally dried at 105 °C for 24 h and stored in a desiccator. For physical activation, approximately 3 g of the original biochar was accurately weighed and placed in a tube furnace, and heated to 800 °C. The total gas flow rate during the activation process was maintained at a constant 200 mL/min. A mass flow controller was used to regulate the flow rates of CO_2 and N_2, while an HPLC pump controlled the flow of water vapor, in order to obtain different volumetric concentrations of CO_2 or steam. The activation duration was set to 2 h, after which the activated biochar samples were cooled under N_2 and stored in sealed desiccators.

To facilitate the differentiation of biochar samples, each sample was labeled according to the treatment method applied. The original acid-washed pine sawdust biochar was designated as BC, while the activated biochar was abbreviated as ABC and distinguished based on the type of activator used: KOH, K_2CO_3, $ZnCl_2$, H_3PO_4, $KMnO_4$, 50 % CO_2, 100 % CO_2, 15 % H_2O and 30 % H_2O. For instance, the KOH activated biochar was labeled as KOH-ABC.

2.3. Online catalytic pyrolysis experiment

As shown in Fig. 1, the online catalytic pyrolysis experiments were conducted using a fixed-bed pyrolysis system. The system consisted of a N_2 gas supply system, a quartz pyrolysis tube heated by an electric furnace, a condensation system for bio-oil collection, and a gas bag for non-condensable gas collection. For each experiment, 0.5 g of activated biochar (ABC) and 0.5 g of acid-washed pine sawdust were placed in the reaction tube in advance as per Fig. 1, separated by silica wool. The furnace was preheated to 500 °C and kept isothermal. The reaction tube was purged with N_2 at 50 mL/min to maintain an inert atmosphere, it was inserted into the furnace, and reacted at 500 °C for 30 min.

Volatiles generated from the pyrolysis of pine sawdust passed through the biochar bed, where catalytic cracking occurred. The resulted vapors were condensed in two gas-washing bottles in an ice bath containing acetone, and the non-condensable gas was collected in a gas bag for analysis. After the experiment finished, the reaction tube was removed from the furnace and cooled under N_2. The used ABC and the

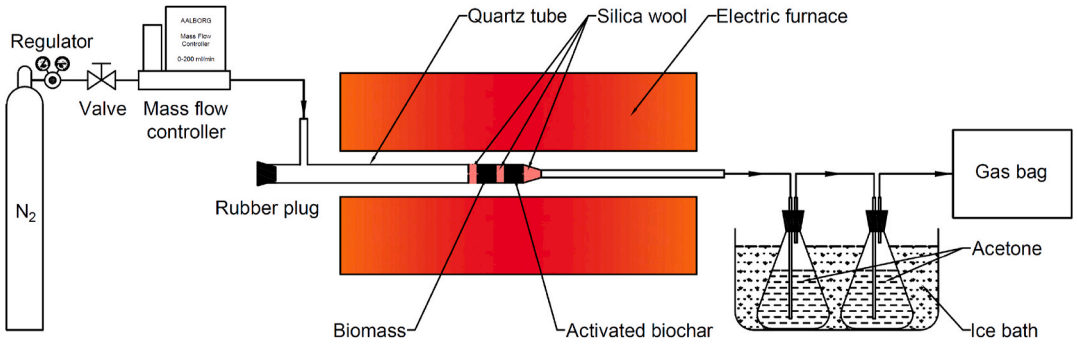

Fig. 1. Schematic diagram of a fixed-bed pyrolysis system.

newly generated biochar (from acid-washed pine sawdust pyrolysis) were both collected and weighed to obtain the weight change and mass yield, respectively. The liquid products, including the bio-oil captured in the acetone bottles and the acetone washings of the pipe lines, were transferred to sample vials and stored at −19 °C for further analysis.

9 ABCs, including KOH-ABC, K_2CO_3-ABC, $ZnCl_2$-ABC, H_3PO_4-ABC, $KMnO_4$-ABC, 50 % CO_2-ABC, 100 % CO_2-ABC, 15 % H_2O-ABC and 30 % H_2O-ABC, were applied for the online catalytic cracking experiment. The ABCs before and after experiment were both collected for further analyses. To ensure the reproducibility of experimental results, each experiment was conducted three times, and the data presented in this study represent the mean values with standard deviations. Additionally, to compare of the catalytic performance of ABC, two experiments of the pyrolysis of pure acid-washed pine sawdust (designated as PY) and the pyrolysis of acid-washed pine sawdust with the addition of BC were also performed at 500 °C.

2.4. Characterization of catalysts and products

2.4.1. Activated biochar (ABC)

The ABC would participate in the catalytic cracking process, resulting in not only being partially consumed (weight loss) but also formation of surface coke (weight gaining), the weight change of ABC before and after reaction was determined by weighing. The physicochemical property of ABC would also change during the reaction, which is closely related to its catalytic performance. The microporosity of ABC before and after reaction was measured using N_2 adsorption-desorption method with a Micromeritics ASAP2020M facility, the specific surface area, pore volume, and pore size distribution of the biochar were calculated using the Brunauer-Emmett-Teller (BET), Barret-Joyner-Halenda (BJH), and t-Plot methods [24]. Raman spectroscopy (Finder Vista) was employed to analyze the chemical structure of the biochar before and after reaction, with a laser wavelength of 532 nm, power of 150 μW, and a spectral resolution of 2 cm^{-1}. The Raman spectra ranging from 1800 to 800 cm^{-1} were later deconvoluted into 9 Gaussian peaks using Peakfit software [25].

2.4.2. Non-condensable gases

The composition of non-condensable gas was analyzed using gas chromatography (GC-9790II, Zhejiang Fuli Analytical Instruments) equipped with TCD and FID detectors [26]. The yields of gas components (N_2, H_2, CO, CO_2, CH_4 and C_{2+} (C_2H_4, C_2H_6, C_3H_6, C_3H_8)) were calculated using the N_2 balance method, based on the known total N_2 volume (50 mL/min × 30 min = 1500 mL) and the gas concentrations (GC test results) [27]. All the mass flow controllers were precisely calibrated before the experiment to ensure the accuracy of the gas flow rates during the experiment. The accuracy of the gas yields calculated would be thus guaranteed.

2.4.3. Bio-oil

The bio-oil was sufficiently condensed in and trapped by acetone solvent. Considering the evaporation of acetone during the process, there might be significant measurement errors to calculate bio-oil yield through direct weighing. Hence, the bio-oil yield in this study would be determined by difference, which would be to use the initial mass of biomass and ABC minus the mass of used ABC and newly generated biochar and the mass of non-condensable gas.

The composition of bio-oil was analyzed using gas chromatography-mass spectrometry (GC-MS, Agilent 6890/5975MS) equipped with an HP-5MS column (30 m × 0.25 mm × 0.25 mm) [28]. The GC injector was set at 275 °C with a split ratio of 50:1. The column temperature was programmed to increase from 40 °C to 200 °C at 5 °C/min, then to 280 °C at 10 °C/min, holding for 3 min. The MS worked under electron ionization (EI) mode at 70 eV with a scanning range from 30 to 300 amu. All the peaks were identified with the NIST11 library, and the peak areas were used for semi-quantitative analysis [29].

3. Results and discussion

3.1. Characterization of activated biochar before and after reaction

3.1.1. Yields of ABC and their weight changes after reaction

Fig. 2 shows the yields of ABC prepared using different activation methods, in which the yield was calculated on a biochar (precursor of ABC) basis. The initial yield of biochar obtained from pyrolysis of pine sawdust was 20.91 wt%. As illustrated in Fig. 2, significant differences were observed in the yields of ABC depending on the activation methods, which might be attributed to the different activation mechanisms. For chemically activated biochar, the yields using KOH, K_2CO_3,

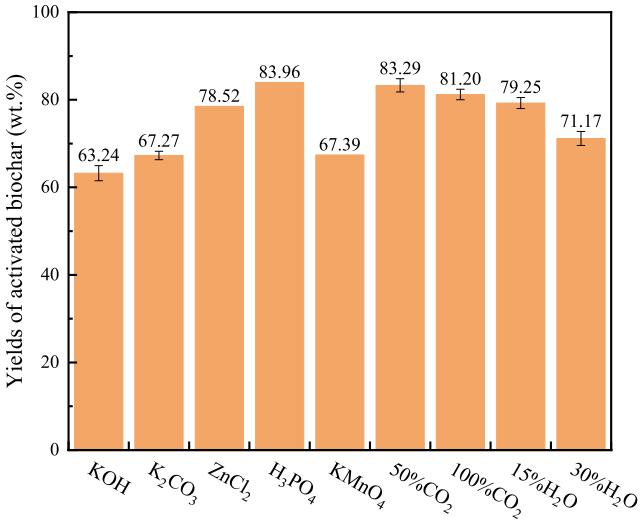

Fig. 2. Yields of activated biochar obtained from different activation methods (on a biochar basis, wt.%).

$ZnCl_2$, H_3PO_4 and $KMnO_4$ activation were 63.24 wt%, 67.27 wt%, 78.52 wt%, 83.96 wt%, and 67.39 wt%, respectively. Whereas biochar activated with alkaline activators, such as KOH and K_2CO_3, exhibited the lowest yields due to their strong corrosive nature. Their reaction with biochar at high temperature aggressively etched the biochar surface, not only generating pores but also reducing the mass yield. $KMnO_4$ activation also gained a low yield of ABC. It might be because that $KMnO_4$ is a strong oxidizing agent, it could be decomposed into K_2MnO_4, MnO_2 and O_2 during activation, and oxidatively etched the carbon matrix to create additional mesopores. Furthermore, K_2MnO_4 would also react with carbon to generate K_2CO_3 and MnO_2, where K_2CO_3 was an important activator and MnO_2 could react with carbon to form MnO, all contributing to further pore formation [30]. Compared to others, $ZnCl_2$ is a neutral metal salt and a commonly used activator with strong abilities in dehydration and degradation of biomass polymers [31]. It would not react directly with biochar during activation, but it would react with dehydrated biomass/biochar to the form large polycyclic aromatic compounds [32], typically resulting in a relatively high yield of ABC. While H_3PO_4 is an acidic activator, which can promote the depolymerization, dehydration, and redistribution of polymers within biomass/biochar, but it has relatively limited impact on pore development, thus a high yield is usually obtained [33].

For physically activated biochar, the yields of CO_2-ABC were higher than those of H_2O-ABC. Specifically, the yields with 50 % CO_2 and 100 % CO_2 activation were 83.29 wt% and 81.20 wt%, respectively, while those with 15 % H_2O and 30 % H_2O activation were 79.25 wt% and 71.17 wt%. Physical activation mainly occurs through the reaction of CO_2 or H_2O with surface carbon atoms, creating pores by consuming carbon, thereby increasing porosity [34]. With the increased concentration of CO_2 or H_2O, the etching effect intensified, leading to lower yields. Also, the reactivity of biochar with H_2O at 800 °C was obviously higher than with CO_2, which explained the lower yields observed for H_2O activation.

Fig. 3 shows the weight changes of different ABCs after catalytic pyrolysis reaction. It can be found that after reaction, the weights of biochar activated by K_2CO_3, KOH, and 30 % H_2O increased, while the weights of biochar activated by $ZnCl_2$, H_3PO_4, $KMnO_4$, 50 % CO_2, 100 % CO_2, and 15 % H_2O decreased. Among them, K_2CO_3-ABC exhibited the largest weight increase, while H_3PO_4-ABC showed the most significant weight loss. In fact, there were two parallel processes affecting the weight of ABC when pyrolytic volatiles passed through the char bed. On the one hand, the biochar participated in the cracking/reforming of volatiles, thereby was partially consumed, resulting in weight loss. On the other hand, the cracking of volatiles on the surface or within the pores of biochar led to coke deposition, which gained weight increase and reduced porosity of biochar. Thus, the overall weight change of biochar could reflect which process dominated during the reaction. In general, more carbon deposition was formed for the biochars activated by K_2CO_3, KOH, and 30 % H_2O during the reaction process, resulting in a weight increase after reaction. As previously shown in Fig. 2, these three activators also produced biochars with relatively low yields, indicating that those active components/structures in biochar that were more prone to consumption during volatiles cracking/reforming process had already been possibly removed during the activation process, which was a possible reason for their observed weight increases after reaction. In addition, although $KMnO_4$-ABC showed low yield (Fig. 2), the strong oxidation characteristic of $KMnO_4$ might retain part of the O-containing groups on the char surface after oxidative activation, thus a significant weight loss was observed due to its self-reforming/gasification during the catalytic cracking (due to CO_2 and H_2O in volatiles). Also, the $KMnO_4$-ABC showed less cracking ability for volatiles during the reaction as proved in the following sections, less coke would be thus formed.

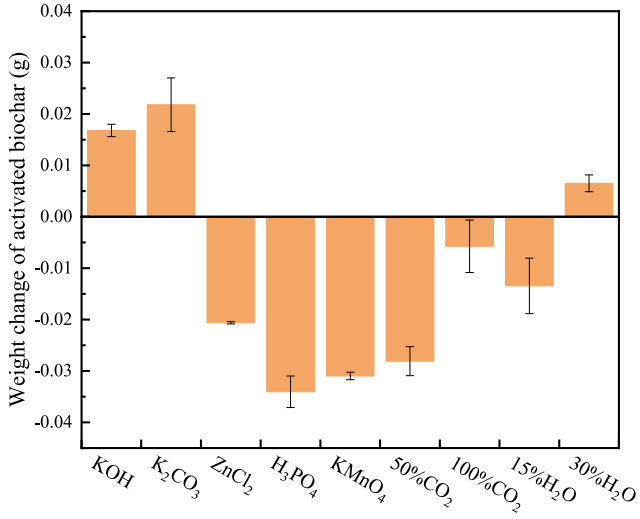

Fig. 3. Weight changes of different activated biochars after catalytic cracking reaction.

3.1.2. Pore structure of activated biochar

Table 1 presents the pore characteristics of various ABCs before and after the catalytic reaction. As shown, significant variations in pore structure were observed among the ABCs produced by different activation methods. KOH exhibited the best activation performance, the resulted KOH-ABC showed a BET surface area of 1677.04 m^2/g and a pore volume of 93.34 × 10^{-2} cm^3/g. It contained abundant micropores and meso/macropores, providing sufficient mass transfer channels and active sites for the cracking of volatiles [35]. The formation of this highly porous structure could be attributed to the rapid penetration of KOH into biochar matrix and the reactions of -OH with biochar to remove carbon atoms on its surface [36]. K_2CO_3 activation demonstrated second, showing a BET surface area of 706.18 m^2/g and a pore volume of 37.38 × 10^{-2} cm^3/g. Here, micropores were dominated, with micropore surface area accounting for 0.88. During activation, K_2CO_3 would be reduced to K_2O and metallic K, releasing CO_2 and CO gases. The generated potassium compounds could penetrate into the biochar matrix, expanding the existing pores and forming new ones [37]. Under current activation conditions, the pore-creating effects of $ZnCl_2$, 15 % H_2O and 30 % H_2O activations were relatively similar, with 30 % H_2O activation being comparatively better. On the contrary, the biochars activated by H_3PO_4, 50 % CO_2 and 100 % CO_2 did not gain desired activation results, especially $KMnO_4$ activation performed the worst with a BET surface area and pore volume of only 173.11 m^2/g and 9.10 × 10^{-2} cm^3/g, respectively. The average pore diameters of all ABCs were relatively consistent, ranging between 2.08 and 2.23 nm.

After reaction, it can be observed that although the changes in pore structure of ABCs varied depending on the activation methods, all biochars experienced a significant reduction in porosity, which could be mainly attributed to the coke deposition from volatiles cracking on biochar surface, blocking or covering the pores. Notably, despite a big reduction of 385.26 m^2/g in BET surface area, KOH-ABC retained a surface area of 1291.78 m^2/g after reaction, which was well above that of other biochars. The reduction in micropore surface area was found to be more significant, the external surface area still had 535.37 m^2/g after reaction, indicating its potential for further use as catalyst for volatiles cracking. Similarly, the 30 % H_2O-ABC also retained a considerable portion of its pore structure after reaction, with a remaining BET surface area of 340.03 m^2/g. The surface area and pore volume of the micropores were both significantly reduced. Other ABCs showed much smaller surface areas and pore volumes after reaction. For instance, the BET surface areas of used biochars activated by K_2CO_3, 15 % H_2O, and $ZnCl_2$ were only 75.18, 65.95, and 18.14 m^2/g, respectively, while the surface areas of the remaining used ABCs were all below 10 m^2/g. The reduction in micropore surface area was more pronounced than that in external surface area for all ABCs. This observation indicated that coke

Table 1
Pore structure characteristics of different activated biochars before and after catalytic cracking reaction.

Activated biochar samples		BET surface area (m^2/g)	t-plot micropore area (m^2/g)	External surface area (m^2/g)	Micropore ratio	Total pore volume ($\times 10^{-2}$ cm^3/g)	t-plot micropore volume ($\times 10^{-2}$ cm^3/g)	External pore volume ($\times 10^{-2}$ cm^3/g)	Average pore width (nm)
Before reaction	KOH	1677.04	1031.86	645.19	0.62	93.34	57.77	35.57	2.23
	K_2CO_3	706.18	618.69	87.49	0.88	37.38	32.47	4.90	2.12
	$ZnCl_2$	493.50	442.00	51.50	0.90	26.32	23.17	3.15	2.13
	H_3PO_4	318.18	280.60	42.05	0.88	16.58	14.73	2.19	2.08
	$KMnO_4$	173.11	131.06	37.58	0.76	9.10	6.91	1.85	2.10
	50 % CO_2	366.99	332.89	34.10	0.91	19.23	17.40	1.82	2.10
	100 % CO_2	368.70	338.80	29.89	0.92	19.53	17.77	1.77	2.12
	15 % H_2O	524.55	482.16	42.39	0.92	27.35	25.25	2.09	2.09
	30 % H_2O	575.89	512.41	63.48	0.89	30.38	26.83	3.55	2.11
After reaction	KOH	1291.78	756.41	535.37	0.59	69.67	41.23	28.44	2.16
	K_2CO_3	75.18	60.89	14.28	0.81	4.09	3.16	0.93	2.18
	$ZnCl_2$	18.14	13.55	4.59	0.75	1.30	0.71	0.59	2.86
	H_3PO_4	2.91	0.38	2.19	0.13	0.35	0.03	0.29	4.81
	$KMnO_4$	2.45	0.27	2.53	0.11	0.31	0.02	0.32	5.08
	50 % CO_2	6.99	2.69	4.30	0.38	0.83	0.15	0.68	4.74
	100 % CO_2	2.84	1.00	1.84	0.35	0.49	0.06	0.44	6.94
	15 % H_2O	65.95	55.48	10.47	0.84	3.69	2.88	0.81	2.24
	30 % H_2O	340.03	290.71	49.32	0.85	18.14	15.29	2.85	2.13

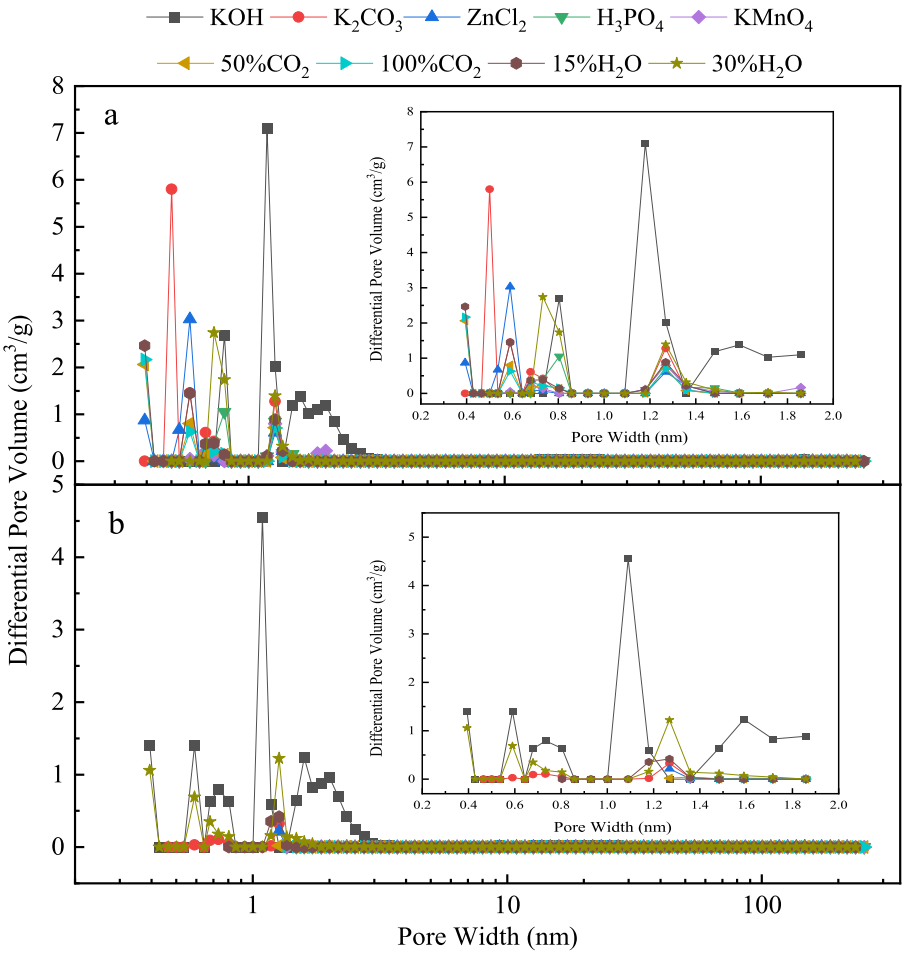

Fig. 4. Pore size distribution of different activated biochars: (a) before reaction, (b) after reaction.

deposition mainly blocked the micropores, which are the main sites for catalytic cracking of volatiles. In contrast, the external pores primarily functioned as mass transfer channels. Combined with the weight change results in Fig. 3, it can be concluded that coke deposition was dominant for K_2CO_3-ABC, KOH-ABC and 30 % H_2O-ABC, as illustrated by their weight increases. Although other ABCs also experienced pore blockages as a result of coke deposition, their weight losses were more substantial because of reaction consumption during the process without a corresponding pore-forming effect.

Fig. 4 shows the pore size distributions of different ABCs before and after the catalytic reaction. From the figure, it can be found that activation methods not only affected in the specific surface area and pore volume of biochars, but also differed their pore size distribution, which was closely related to their catalytic cracking performances. After activation, the pore distribution of biochars was relatively narrow, primarily ranging between 0.4 and 3 nm. K_2CO_3-ABC and KOH-ABC exhibited more developed pore structures. Comparatively, the pores of K_2CO_3-ABC were smaller, most of the pores were concentrated around 0.5 nm, along with additional distributions at around 0.59, 0.68, 0.73, and 1.27 nm. While KOH-ABC exhibited its primary pore size distribution around 1.18 nm, with additional pores distributed at 0.8 nm and 1.27–3 nm. The 30 % H_2O-ABC exhibited a major pore distribution at 0.73–0.80 nm, with a smaller distribution around 1.27 nm. In comparison, the 15 % H_2O-ABC showed smaller pores, due to its relatively lower degree of activation. The differences between two CO_2-ABCs were insignificant, probably because of their lower degree of activation. $ZnCl_2$-ABC also exhibited a well-developed pore structure, with most pores concentrated around 0.59 nm and additional distributions at 0.39 and 1.27 nm. The other ABCs contained fewer pores, primarily smaller than 0.8 nm.

After reaction, the pore structures of ABCs were all significantly reduced. Only KOH-ABC still showed quite a lot of pore structures, followed by 30 % H_2O-ABC. In contrast, only a few remaining pores were observed for K_2CO_3-ABC, 15 %H_2O-ABC, and $ZnCl_2$-ABC, while the pore structures of other ABCs were almost entirely disappeared, consistent with the findings in Table 1. Overall, the pores smaller than 0.68 nm in ABCs were almost entirely blocked by coke deposition during the reaction, while the pores larger than 0.68 nm were reduced in size. For instance, the pore size distributions of KOH-ABC and 30 % H_2O-ABC shifted toward smaller diameters after the reaction. This suggested that the micropores larger than 0.68 nm, particularly those greater than 1 nm, are more resistant to blockage during the catalytic cracking of volatiles. Therefore, controlling the pore size distribution of ABC by minimizing the fraction of ultra-micropores (<0.68 nm) is crucial for maintaining its catalytic activity.

3.1.3. Chemical structure of activated biochar

Table 2 shows the total Raman areas (1800-800 cm^{-1}) and the band ratios of I_D/I_G of different ABCs before and after the catalytic cracking reaction. The total Raman area can reflect the abundance of O-containing functional groups on biochar surface as these groups enhance Raman intensity [38]. The ratio of I_D/I_G indicates the number of defects on biochar surface. In Tables 2 and it can be observed that the total Raman areas of the ABCs varied depending on the activation methods, indicating the altered chemical structures during the activation process [39]. Different activators interacted with biochar through distinct mechanisms, leading to the variations in the amount and types of O-containing functional groups on the char surface. These functional groups, including carboxylic and hydroxyl groups, could serve as chemical adsorption active sites for volatile molecules during catalytic cracking (such as through hydrogen bond) [10,40]. The differences in the amount of O-containing functional groups would affect the catalytic performance of ABC in cracking volatiles/bio-oil. This suggested that the biochars activated by KOH, K_2CO_3 and 30 % H_2O might exhibit better initial catalytic activity. After reaction, the total Raman areas of all ABCs decreased substantially, further confirming that O-containing functional groups acted as active sites for the cracking reactions and were partially consumed during the process. And KOH-ABC, K_2CO_3-ABC and 30 % H_2O-ABC might still retain some activity after reaction. The I_D/I_G ratios also decreased after reaction, indicating a reduction in defects on biochar surface. These defects included heteroatom O-induced defects (e.g., O-containing functional groups), edge defects, and carbon atom vacancies in carbon structures. Such defects were typically highly reactive and could serve as active sites for catalytic cracking. The decrease in I_D/I_G ratio could be attributed to on the one hand the aforementioned consumption of O-containing functional groups, and on the other hand, the transformation or consumption of reactive carbon defects during the reaction (via interactions with volatiles through π-π stacking of aromatic rings) [11].

Table 2
Total Raman area (1800-800 cm^{-1}) and ratio of band areas I_D/I_G from different activated biochars.

ABC	Total Raman area		I_D/I_G	
	Before reaction	After reaction	Before reaction	After reaction
KOH	772002	554447	1.11	1.01
K_2CO_3	876460	550352	0.98	0.88
$ZnCl_2$	745824	376735	1.21	0.90
H_3PO_4	523988	451412	1.11	0.83
$KMnO_4$	506463	333332	1.11	1.00
50 %CO_2	744972	380162	1.16	0.97
100 %CO_2	603392	492909	1.00	0.97
15 %H_2O	594712	490143	1.09	1.06
30 %H_2O	792391	533442	1.11	1.06

3.2. Pyrolysis product yield

The ABCs prepared using different activation methods were applied for the online catalytic cracking of volatiles from pine sawdust pyrolysis, and their catalytic performance on bio-oil upgrading was analyzed. The pyrolysis experiments with pure pine sawdust (PY, without catalyst addition) and with the addition of non-activated biochar (BC) respectively were also conducted for comparison. The mass yield distributions of the pyrolysis products are presented in Fig. 5.

As shown in Fig. 5, the biochar yield from the pyrolysis of pure pine sawdust (PY) was 29.89 wt%. In the catalytic cracking experiments with different biochar samples, as only the volatiles generated from PY interacted with the adjacent activated biochar layer, while the freshly generated biochar did not contact or react with it, the freshly generated

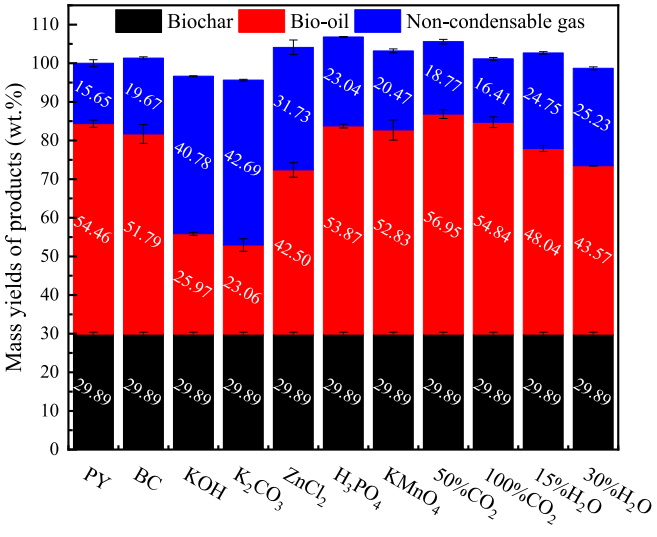

Fig. 5. Mass yields of pyrolysis products from online catalytic cracking of pine sawdust volatiles over different activated biochars.

biochar yield in these experiments was thus assumed to be the same as that of PY, maintaining a value of 29.89 wt%. The yields of bio-oil and non-condensable gas from PY were 54.46 wt% and 15.65 wt%, respectively. Using biochar to catalytically crack volatiles, the decomposition of these compounds inevitably produced small gaseous molecules, such as CO, CO_2 and CH_4, resulting in a reduction in bio-oil yield and an increase in non-condensable gas yield. The extent of these changes could reflect the depth and efficiency of the cracking process facilitated by the biochar. For instance, when BC was used, the bio-oil yield decreased to 51.79 wt%, while the non-condensable gas yield increased to 19.67 wt %. As discussed previously, the catalytic cracking process involved two parallel phenomena: (1) biochar, including both BC and ABC, participated in the reactions, resulting in partial consumption to form more gaseous products; and (2) coke deposition occurred as volatiles cracking on biochar surface or within its pores, leading to a weight increase in biochar and a total yield reduction in pyrolysis products. As a result, the total yields of pine sawdust pyrolysis products presented in Fig. 5 exceeded 100 wt% in some cases, and fell below 100 wt% in others (e.g., with KOH-ABC, K_2CO_3-ABC and 30 % H_2O-ABC). These observations were consistent with the weight change results of the ABCs after reaction, as shown in Fig. 3.

As previously mentioned, the changes in the yields of bio-oil and non-condensable gas could reflect the extent/depth of volatile cracking. From Fig. 5, it can also be observed that different ABCs exhibited distinct catalytic cracking performance on volatiles. In general, compared to PY, the addition of all ABCs increased the yield of non-condensable gas, indicating that the interactions between volatiles and biochar did occur [4]. More specifically, KOH-ABC and K_2CO_3-ABC demonstrated the highest volatiles cracking performance, with bio-oil yields reduced to 25.97 wt% and 23.06 wt%, respectively, and non-condensable gas yields increased to 40.78 wt% and 42.69 wt%. $ZnCl_2$-ABC and 30 % H_2O-ABC exhibited moderate cracking abilities, resulting in bio-oil yields of 42.50 wt% and 43.57 wt%, with corresponding non-condensable gas yields of 31.73 wt% and 25.23 wt%. In comparison, the other ABCs displayed relatively poor catalytic cracking performance on volatiles. Combining with the porosity results shown in Tables 1 and it can be found that the cracking performance of biochars showed a positive correlation with their BET surface areas and pore volumes [35,41]. Biochars activated with KOH, K_2CO_3, $ZnCl_2$, and 30 % H_2O, which had relatively higher surface areas and pore volumes, provided more contact areas and reaction places for the cracking of volatiles. In contrast, biochars activated with H_3PO_4, $KMnO_4$, 50 % CO_2 and 100 % CO_2, which exhibited less developed pore structures, showed inferior catalytic cracking performance. However, the relationship between pore structure and cracking performance was not strictly linear. For example, K_2CO_3-ABC exhibited deeper cracking of volatiles than KOH-ABC, as a lower bio-oil yield and higher non-condensable gas yield were obtained, despite its relatively lower surface area and pore volume. But on the other hand, it can be also observed that K_2CO_3-ABC showed a more significant reduction in its surface area (631.00 m^2/g) and more coke formation on char surface (illustrated by its highest weight increase in Fig. 3) after reaction, indicating such deeper cracking of volatiles on its surface. However, 50 % CO_2-ABC and 100 % CO_2-ABC only showed very limited catalytic cracking performances on volatiles, which was not consistent with some results reported in the literature [10]. This discrepancy might be attributed to the difference in pore structure of CO_2-ABCs used in the study, the pore structure of the char was not well activated under the current activation condition, that might be the possible reason.

3.3. Composition and volumetric yield of non-condensable gas

Fig. 6 shows the composition and volumetric yield of non-condensable gas from the online catalytic cracking of volatiles from pine sawdust pyrolysis using different ABCs. For comparison, the results from the pyrolysis of pure pine sawdust (PY) and the catalytic cracking experiments with non-activated biochar (BC) are also included.

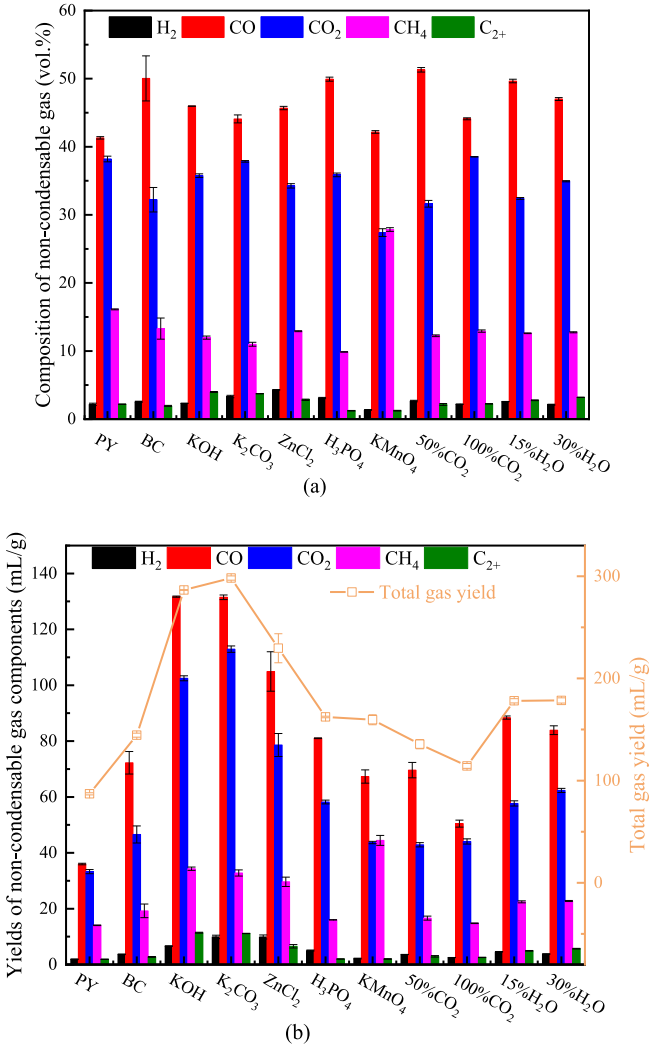

Fig. 6. Composition and yield of non-condensable gas from online catalytic cracking of volatiles from pine sawdust pyrolysis over different activated biochars: (a) gas composition, (b) gas yields.

As shown in Fig. 6a, the main gases generated from PY were CO, CO_2 and CH_4, with small amounts of H_2 and C_{2+} gases. In comparison to PY, the addition of different biochars for catalytic cracking altered the composition of non-condensable gas. In general, the CO content increased, while the CO_2 content decreased. Additionally, the CH_4 content decreased, whereas the contents of H_2 and C_{2+} increased slightly (except for $KMnO_4$-ABC). It implied that the deoxygenation of bio-oil over biochar was mainly in the form of CO, which was accompanied by the dehydrogenation and dealkylation reactions as well. However, it should be also noted that a reduction in the content of a gas component did not necessarily indicate a decrease in its yield; it only reflected the relative yield change during the process. The varied non-condensable gas compositions for different ABCs further highlighted their differences in cracking abilities. Among the biochars, $KMnO_4$-ABC exhibited a distinct behavior, a substantial increase in CH_4 content and a decrease in H_2 and C_{2+} contents were observed, suggesting a much stronger ability for the cleavage of methyl (-CH_3) or methoxy (-O-CH_3) side chains over $KMnO_4$-ABC during the cracking process.

As shown in Fig. 6b, compared to PY, the addition of BC and ABCs all significantly increased the yield of non-condensable gas, indicating that biochar did promote the cracking of volatiles. The yields of CO and CO_2 increased substantially, accompanied by a noticeable increase in CH_4 yield, as well as a moderate increase in the yields of H_2 and C_{2+} [6]. The

deoxygenation of bio-oil over different biochars was mainly in the form of CO and CO_2. Notably, the increase in CO yield was more significant, aligning with the results shown in Fig. 6a. In addition, all biochars demonstrated the abilities of dehydrogenation and dealkylation, contributing to the increased yields of H_2 and C_{2+}. From the perspective of non-condensable gas yields, BC already exhibited some deoxygenation capability, as evidenced by the increased yields of CO and CO_2 compared to PY. KOH-ABC and K_2CO_3-ABC showed the highest deoxygenation performance, with the yields of CO and CO_2 increasing by 2–3 times compared to PY. The yields of H_2, CH_4, and C_{2+} also increased significantly. $ZnCl_2$-ABC showed moderate deoxygenation performance, followed by 15 % H_2O-ABC and 30 % H_2O-ABC. These results are consistent with those shown in Fig. 5, where the deoxygenation ability of different ABCs corresponded to the extent/depth of volatiles cracking. Furthermore, during the catalytic cracking of volatiles, the biochar participated in the reaction with part of its weight being lost/consumed and going into the gas phase, contributing to the increased yield of non-condensable gases, such as H_3PO_4-ABC, $KMnO_4$-ABC, 50 % CO_2-ABC and 100 % CO_2-ABC (Fig. 3). Among them, $KMnO_4$-ABC exhibited the highest ability to cleave methyl (-CH_3) or methoxy (-O-CH_3) groups, resulting in the highest CH_4 yield.

3.4. Composition and distribution of bio-oils

Fig. 7 presents the composition and color of bio-oil obtained from the online catalytic cracking of volatiles from pine sawdust pyrolysis using different ABCs. The bio-oils from the pyrolysis of pure pine sawdust (PY) and the online catalytic cracking of volatiles over non-activated biochar (BC) are also presented for comparison. It is important to note that only part of the components in bio-oil were detected by GC-MS, primarily those lighter fractions, while many heavy fractions or low-abundance compounds in bio-oil might not be detected or identified. Additionally, the composition of bio-oil was semi-quantitatively expressed as the peak area percentage. Given the significant differences in response factors among various compounds, these values did not reflect the mass content of each component. Furthermore, the liquid levels shown in the sample vials in Fig. 7b did not represent the bio-oil yields. They were only related to the amount of acetone solvent used during the process (for bio-oil capture and washing). While the mass yield of bio-oil could be found in Fig. 5.

As shown in Fig. 7a, the composition of bio-oil derived from pine sawdust pyrolysis was highly complex, consisting primarily of linear acids, linear carbonyls (e.g., ketones, aldehydes, and esters), furans, cyclopentanones, anhydrosugars, phenols and other aromatics. The bio-oil from PY contained a large proportion of anhydrosugars (71.44 %), along with a certain amount of carbonyls (10.37 %) and phenols or aromatics (12.72 %). BC exhibited limited cracking ability for volatiles, the resulted bio-oil was still dominated by anhydrosugars (73.55 %). Mainly linear acids and carbonyls were cleaved (forming CO and CO_2, as shown in Fig. 6), while the content of furans increased slightly. KOH-ABC and K_2CO_3-ABC were most effective in the deoxygenation of bio-oil (consistent with the results shown in Figs. 5 and 6), with the bio-oil for KOH-ABC containing only furans (10.43 %) and phenols and aromatics (89.57 %). Similarly, the bio-oil for K_2CO_3-ABC consisted of linear carbonyls (17.01 %), furans (10.17 %), and phenols and aromatics (72.83 %). The deep deoxygenation of bio-oil resulted in a significant reduction in its yield (as shown in Fig. 5), but the remaining components were more concentrated, with significantly improved selectivity toward phenols and aromatics, increasing the value of bio-oil. During biomass pyrolysis, the holocellulose would undergo depolymerization and dehydration to form various anhydrosugars (such as levoglucosan). The depolymerized sugar units (e.g., pyran ring unit) could further experience ring-opening reactions (e.g., cleavage of C-C bonds) to generate linear acids and carbonyls (such as aldehydes, ketones, and esters) [42, 43]. The phenols and aromatics in bio-oil were not only derived from the depolymerization of lignin, but could also be formed through the dehydration and cyclization/aromatization of light linear molecules (such as acids and carbonyls) [44].Similarly, furans and cyclopentenones could also be generated through decarboxylation/decarbonylation and dehydration of light linear molecules for

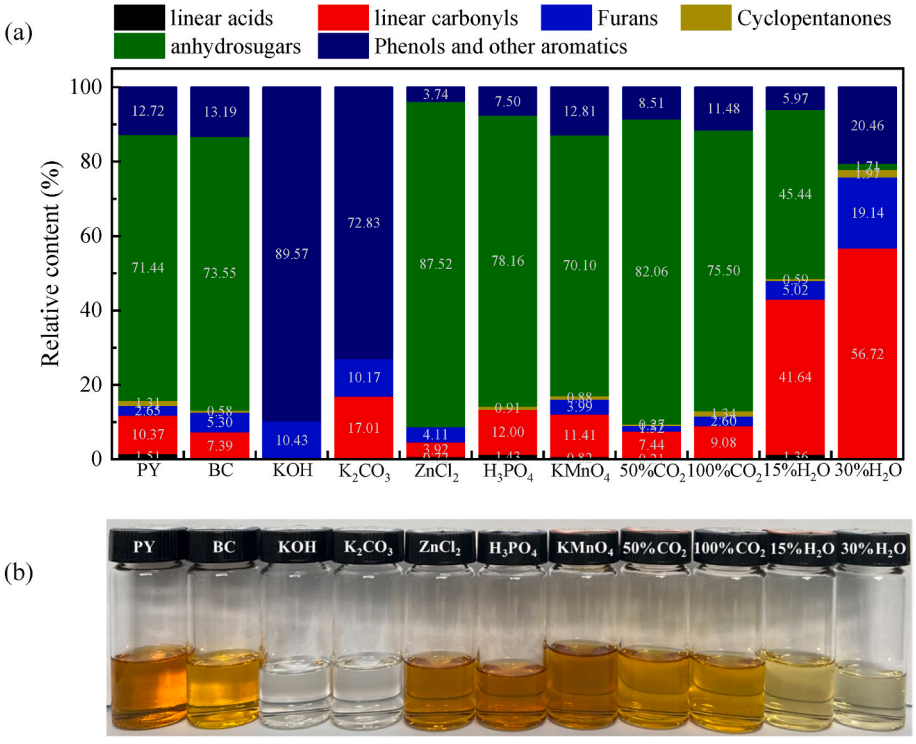

Fig. 7. Bio-oil obtained from online catalytic cracking of volatiles from pine sawdust pyrolysis over different activated biochars: (a) composition of bio-oil detected by GC-MS, and (b) colors of bio-oil.

recyclization. KOH-ABC and K_2CO_3-ABC, with their well-developed porous structures and abundant surface O-containing functional groups, showed significantly enhanced catalytic cracking activities, the deoxygenation rate of bio-oil was largely improved, with the removal of O from linear acids and carbonyls, and anhydrosugars in bio-oil in the form of CO, CO_2 (via decarbonylation and decarboxylation, as illustrated in Fig. 6b), and H_2O (via dehydration). On the highly active biochar surfaces, linear acids could further undergo dehydration and aromatization reactions to generate aromatic hydrocarbons [44]. Additionally, anhydrosugars may undergo ring-opening, dehydration, and cyclization reactions to form more furans and aromatics as well [15]. The highly porous nature of KOH-ABC and K_2CO_3-ABC would provide enough reaction spaces or active sites for the volatiles cracking over biochar surface, the deep deoxygenation of bio-oil was thus achieved with high selectivity of phenols and aromatics formation during the process [41]. The bio-oil obtained with $ZnCl_2$-ABC, H_3PO_4-ABC, 50 % CO_2-ABC and 100 % CO_2-ABC exhibited some enrichment in anhydrosugars compared to PY, suggesting their cracking effect on linear acids, carbonyls, and phenols and aromatics over ABCs. However, their deoxygenation abilities were generally lower than those of KOH-ABC and K_2CO_3-ABC due to their lower porosity. $KMnO_4$-ABC showed limited cracking ability, with relatively minor changes in bio-oil composition. H_2O-ABCs exhibited relatively good catalytic cracking performance, the content of anhydrosugars in bio-oil decreased significantly, more linear carbonyls (41.64 % for 15 % H_2O-ABC) were formed due to the ring-opening of these anhydrosugar in volatiles on char surface. As the activation level increased (30 % H_2O-ABC), the enhancement of the ring-opening reactions became more pronounced, resulting in a higher yield of carbonyls (56.72 %). More furans (19.14 %) and phenols and aromatics (20.46 %) were also formed through further cyclization. It is important to note that, in this study, the catalytic cracking activities of different ABCs over pyrolytic volatiles varied significantly, mainly depending on the activation methods. However, these differences should be specific to the physicochemical properties of the biochars produced under the carbonization and activation conditions employed in this study. Modifying the physical and chemical surface structures of ABC by adjusting the activation parameters would potentially yield different catalytic behaviors and trends.

As shown in Fig. 7b, the bio-oil obtained from catalytic cracking of volatiles over different ABCs exhibited notable differences in apparent color. The original bio-oil (PY) dissolved in acetone appeared predominantly brown. In contrast, the bio-oils produced using KOH-ABC and K_2CO_3-ABC were nearly colorless. The bio-oils for H_2O-ABCs also showed a significant lightning in color, with a more pronounced color change for the bio-oil with 30 % H_2O-ABC. The bio-oils from $ZnCl_2$-ABC, H_3PO_4-ABC and $KMnO_4$-ABC showed minimal color changes, while the bio-oils with CO_2-ABCs were slightly lighter in color. The color change of the bio-oil reflected, to some extent, the variations in its composition, particularly its anhydrosugar content, which aligned with the results shown in Fig. 7a. Overall, the bio-oils produced with KOH-ABC and K_2CO_3-ABC appeared to be purer and of higher quality.

3.5. Possible mechanism for high selective phenols and aromatics formation over activated biochar

From the above discussions, the deep deoxygenation of bio-oil over ABC mainly forms phenols and aromatics. The high selective formation of phenols and aromatics over ABC can be summarized into 4 major pathways (Fig. 8): (1) the depolymerization of lignin in biomass to directly form phenols (further dehydration and dealkoxylation to form aromatics), as the basic units (monomers) of lignin are phenolic derivatives, including guaiacyl (G), syringyl (S), and p-hydroxyphenyl (H); (2) the decarboxylation/decarbonylation and dehydration of light linear compounds (e.g., acids, ketones, aldehydes) and subsequent cyclization/aromatization; (3) the ring-opening (C-C cleavage) of sugar units (e.g., anhydrosugars from depolymerization of holocellulose) to firstly form light linear compounds and followed with pathway (2); (4) the ring-opening (C-O cleavage) of anhydrosugars and subsequent dehydration and rearrangement/recyclization.

The presence of ABC mainly enhances the reaction pathways (2)–(4) to form more phenols and aromatics. The porous structure and O-containing surface functional groups in ABC are both important for the catalytic cracking/deoxygenation of volatiles/bio-oil. The abundant pores of char can provide sufficient mass transfer channels and reaction spaces for the volatiles cracking, while the O-containing groups (e.g., -COO and -OH groups) act as the active sites for chemosorption and reactions [10]. Comparatively, the pore structure of ABC plays a dominated role during the bio-oil deoxygenation, as a high BET surface area of biochar would provide more contact surfaces/reaction spaces and effective active sites for the bio-oil cracking [41], especially for those micro- and meso-pores larger than 0.68 nm (mainly 1–3 nm) with less likely being blocked by coke during the reaction. Meanwhile, the BET surface area determines the depth of bio-oil cracking/deoxygenation, as evidenced by the varied cracking abilities for different ABCs. For instance, H_3PO_4-ABC, $KMnO_4$-ABC and CO_2-ABC with less BET surface areas exhibited low cracking abilities, resulting in high content of anhydrosugars and low content of phenols and aromatics in bio-oil. H_2O-ABC with medium BET surface area showed moderate cracking ability, resulting in much lower higher content of anhydrosugars and higher contents of carbonyls and phenols and aromatics. While KOH-ABC and K_2CO_3-ABC with high BET surface area induced deep cracking and deoxygenation of bio-oil through reaction pathways (2)–(4), high selectivity formation of phenols and aromatics was thus achieved. In other words, highly porous structure of ABC would allow

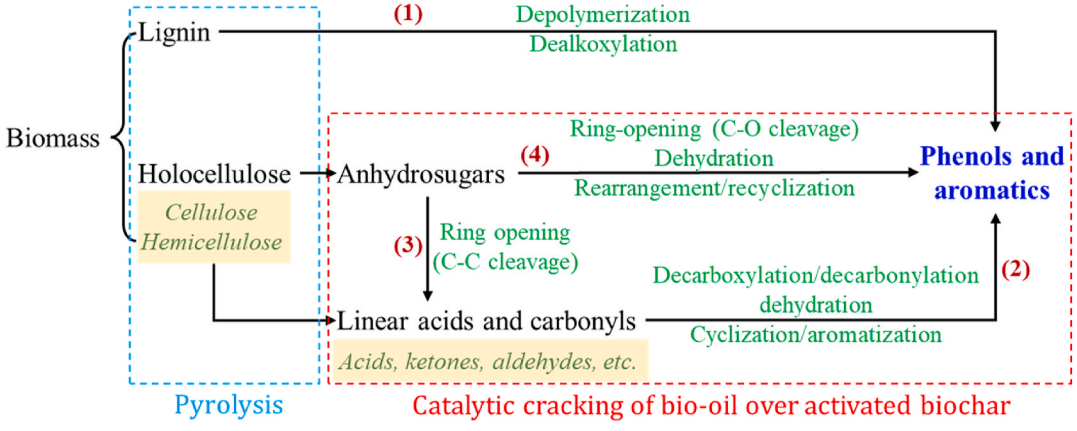

Fig. 8. Formation mechanism of phenols and aromatics during online catalytic cracking of volatiles from pine sawdust pyrolysis over activated biochar.

the reactions involved in the above pathways to thoroughly proceed, while less BET surface area might terminate the cracking process earlier before sufficiently deoxygenation.

4. Conclusion

This study clearly shows the importance of pore and chemical structures of ABC on the catalytic deoxygenation of bio-oil. Activation methods significantly affected the pore characteristics and surface chemical structure of biochar as well as its corresponding cracking/deoxygenation performance. The ABC participated in the reactions, leading to the reduced surface O-containing functional groups/defects (being consumed) and porosity (being blocked by coke formation). The ultra-micropores less than 0.68 nm were especially prone to complete blockage by coke deposition, an appropriate distribution of micropores and mesopores (e.g., 1–3 nm) was preferable to retain its catalytic activity. Bio-oil was deoxygenated over biochar surface primarily in the form of CO (predominantly), CO_2 and H_2O, along with dehydrogenation (forming H_2) and dealkylation (forming CH_4 and C_{2+}) reactions. The O-containing surface groups of ABCs acted as active sites during the bio-oil cracking, but their porous structures played a dominated role during bio-oil deoxygenation, the depth/degree of bio-oil cracking/deoxygenation was found to be determined by the BET surface areas obtained from different activation methods. The KOH-ABC and K_2CO_3-ABC with high porosities and appropriate pore size distribution could deeply deoxygenate bio-oil to selectively form phenols and aromatics. The H_2O-ABC with medium BET surface area exhibited moderate deoxygenation ability, resulting in more carbonyls formation. In contrast, $ZnCl_2$-ABC, H_3PO_4-ABC, $KMnO_4$-ABC and CO_2-ABC with less porosities exhibited low cracking/deoxygenation abilities. The possible cracking/deoxygenation reaction mechanism over ABC was also summarized. This study establishes the relationship among the activation methods, the physicochemical structures of biochar and their bio-oil catalytic cracking performances, it can provide guidance for the optimization of biochar activation strategies for bio-oil deoxygenation.

CRediT authorship contribution statement

Derui Yang: Writing – original draft, Investigation, Formal analysis, Data curation. **Wojciech Jerzak:** Writing – review & editing, Supervision. **Yusuf Makarfi Isa:** Writing – review & editing. **Xing Xie:** Writing – review & editing, Supervision, Resources. **Dan Lin:** Writing – review & editing, Supervision. **Haiping Yang:** Writing – review & editing, Supervision. **Shihong Zhang:** Writing – review & editing, Supervision. **Youjian Zhu:** Writing – review & editing, Supervision. **Bin Li:** Writing – review & editing, Supervision, Resources, Methodology, Funding acquisition, Conceptualization.

Declaration of competing interest

The authors declare that they have no known competing financial interests or personal relationships that could have appeared to influence the work reported in this paper.

Acknowledgements

The authors would like to express their sincere thanks for the financial supports from the National Natural Science Foundation of China (52276196), the Foundation of State Key Laboratory of Coal Combustion (FSKLCCA2508), and the High-level Talent Foundation of Anhui Agricultural University(rc412307).

Appendix A. Supplementary data

Supplementary data to this article can be found online at https://doi.org/10.1016/j.energy.2025.136037.

Data availability

Data will be made available on request.

References

[1] Li B, Song M, Xie X, Wei J, Xu D, Ding K, Huang Y, Zhang S, Hu X, Zhang S, Liu D. Oxidative fast pyrolysis of biomass in a quartz tube fluidized bed reactor: effect of oxygen equivalence ratio. Energy 2023;270:126987.
[2] Zhang S, Zou K, Li B, Shim H, Huang Y. Key considerations on the industrial application of Lignocellulosic biomass pyrolysis toward carbon neutrality. Engineering 2023;29:35–8.
[3] Li B, Zhao L, Xie X, Lin D, Xu H, Wang S, Xu Z, Wang J, Huang Y, Zhang S, Hu X, Liu D. Volatile-char interactions during biomass pyrolysis: effect of char preparation temperature. Energy 2021;215:119189.
[4] Li B, Huang H, Xie X, Wei J, Zhang S, Hu X, Zhang S, Liu D. Volatile-char interactions during biomass pyrolysis: effects of AAEMs removal and KOH addition in char. Renew Energy 2023;219:119459.
[5] Li B, Liu D, Lin D, Xie X, Wang S, Xu H, Wang J, Huang Y, Zhang S, Hu X. Changes in biochar functional groups and its reactivity after volatile–char interactions during biomass pyrolysis. Energy Fuels 2020;34:14291–9.
[6] Hu J, Si Y, Yang H, Shao J, Wang X, Lei T, Agblevor FA, Chen H. Influence of volatiles-char interactions between coal and biomass on the volatiles released, resulting char structure and reactivity during co-pyrolysis. Energy Convers Manag 2017;152:229–38.
[7] Mahmood F, Ali M, Khan M, Mbeugang CFM, Isa YM, Kozlov A, Penzik M, Xie X, Yang H, Zhang S, Li B. A review of biochar production and its employment in synthesizing carbon-based materials for supercapacitors. Ind Crop Prod 2025;227:120830.
[8] Marousek J, Gavurova B, Marouskova A. Cost breakdown indicates that biochar production from microalgae in central Europe requires innovative cultivation procedures. Energy Nexus 2024;16:100335.
[9] Liu Y, Paskevicius M, Wang H, Parkinson G, Veder J-P, Hu X, Li C-Z. Role of O-containing functional groups in biochar during the catalytic steam reforming of tar using the biochar as a catalyst. Fuel 2019;253:441–8.
[10] Liu S, Wu G, Gao Y, Li B, Feng Y, Zhou J, Hu X, Huang Y, Zhang S, Zhang H. Understanding the catalytic upgrading of bio-oil from pine pyrolysis over CO_2-activated biochar. Renew Energy 2021;174:538–46.
[11] Huang Y, Liu S, Akhtar MA, Li B, Zhou J, Zhang S, Zhang H. Volatile–char interactions during biomass pyrolysis: understanding the potential origin of char activity. Bioresour Technol 2020;316:123938.
[12] Zou R, Qian M, Wang C, Mateo W, Wang Y, Dai L, Lin X, Zhao Y, Huo E, Wang L, Zhang X, Kong X, Ruan R, Lei H. Biochar: from by-products of agro-industrial lignocellulosic waste to tailored carbon-based catalysts for biomass thermochemical conversions. Chem Eng J 2022;441:135972.
[13] Anto S, Sudhakar MP, Ahamed TS, Samuel MS, Mathimani T, Brindhadevi K, Pugazhendhi A. Activation strategies for biochar to use as an efficient catalyst in various applications. Fuel 2021;285:119205.
[14] Sajjadi B, Chen W-Y, Egiebor NO. A comprehensive review on physical activation of biochar for energy and environmental applications. Rev Chem Eng 2019;35:735–76.
[15] Zhang Y, Lei H, Yang Z, Duan D, Villota E, Ruan R. From glucose-based carbohydrates to phenol-rich bio-oils integrated with syngas production via catalytic pyrolysis over an activated carbon catalyst. Green Chem 2018;20:3346–58.
[16] Shen W, Cao B, Mu M, Yuan C, Li C, Hu X, Wang S, Abomohra A. Monophenols recovery by catalytic pyrolysis of waste sawdust over activated biochar from the brown macroalgae Hizikia fusiformis: mechanism and life-cycle assessment. J Anal Appl Pyrolysis 2023;169:105798.
[17] González-García P. Activated carbon from lignocellulosics precursors: a review of the synthesis methods, characterization techniques and applications. Renew Sustain Energy Rev 2018;82:1393–414.
[18] Korus A, Gutierrez J-P, Szlęk A, Jagiello J, Hornung A. Pore development during CO_2 and H_2O activation associated with the catalytic role of inherent inorganics in sewage sludge char and its performance during the reforming of volatiles. Chem Eng J 2022;446:137298.
[19] Geczo A, Giannakoudakis DA, Triantafyllidis K, Elshaer MR, Rodríguez-Aguado E, Bashkova S. Mechanistic insights into acetaminophen removal on cashew nut shell biomass-derived activated carbons. Environ Sci Pollut Control Ser 2020;28:58969–82.
[20] Wu Y, Cheng H, Pan D, Zhang L, Li W, Song Y, Bian Y, Jiang X, Han J. Potassium hydroxide-modified algae-based biochar for the removal of sulfamethoxazole: sorption performance and mechanisms. J Environ Manag 2021;293:112912.
[21] Pallarés J, González-Cencerrado A, Arauzo I. Production and characterization of activated carbon from barley straw by physical activation with carbon dioxide and steam. Biomass Bioenergy 2018;115:64–73.
[22] Zheng Y, Wang J, Li D, Liu C, Lu Y, Lin X, Zheng Z. Insight into the KOH/$KMnO_4$ activation mechanism of oxygen-enriched hierarchical porous biochar derived from biomass waste by in-situ pyrolysis for methylene blue enhanced adsorption. J Anal Appl Pyrolysis 2021;158:105269.
[23] Li B, Tang J, Xie X, Wei J, Xu D, Shi L, Ding K, Zhang S, Hu X, Zhang S, Liu D. Char structure evolution during molten salt pyrolysis of biomass: effect of temperature. Fuel 2023;331:125747.

[24] Khan N, Ahmad A, Sharma V, Saha AK, Pandey A, Chaturvedi Bhargava P. An integrative study for efficient removal of hazardous azo dye using microbe-immobilized cow dung biochar in a continuous packed bed reactor. Renew Energy 2022;200:1589–601.
[25] Li X, Hayashi J-i, Li C-Z. FT-Raman spectroscopic study of the evolution of char structure during the pyrolysis of a Victorian brown coal. Fuel 2006;85:1700–7.
[26] Magoua Mbeugang CF, Mahmood F, Ali M, Tang J, Li B. H_2-rich syngas production and tar removal over biochar-supported Ni-Fe bimetallic catalysts during catalytic pyrolysis-gasification of biomass. Renew Energy 2025;243:122547.
[27] Lu T, Lin D, Isa YM, Kozlov A, Penzik M, Xie X, Zhang S, Yang H, Li B. Influence of oxygen equivalence ratio on biochar oxidation characteristics under biomass oxidative pyrolysis conditions in a fluidized-bed reactor. J Energy Inst 2025;119:101995.
[28] Khan N, Chowdhary P, Ahmad A, Shekher Giri B, Chaturvedi P. Hydrothermal liquefaction of rice husk and cow dung in mixed-bed-rotating pyrolyzer and application of biochar for dye removal. Bioresour Technol 2020;309:123294.
[29] Ali M, Mahmood F, Magoua Mbeugang CF, Tang J, Xie X, Li B. Molten chloride salt pyrolysis of biomass: effects of temperature and mass ratio of molten salt to biomass. Energy 2025;316:134634.
[30] Qiu D, Guo N, Gao A, Zheng L, Xu W, Li M, Wang F, Yang R. Preparation of oxygen-enriched hierarchically porous carbon by $KMnO_4$ one-pot oxidation and activation: mechanism and capacitive energy storage. Electrochim Acta 2019;294:398–405.
[31] Olivares-Marin M, Fernandez-Gonzalez C, Macias-Garcia A, Gomez-Serrano V. Preparation of activated carbon from cherry stones by chemical activation with $ZnCl_2$. Appl Surf Sci 2006;252:5967–71.
[32] Gundogdu A, Duran C, Senturk HB, Soylak M, Imamoglu M, Onal Y. Physicochemical characteristics of a novel activated carbon produced from tea industry waste. J Anal Appl Pyrolysis 2013;104:249–59.
[33] Abdelnaeim MY, El Sherif IY, Attia AA, Fathy NA, El-Shahat MF. Impact of chemical activation on the adsorption performance of common reed towards Cu(II) and Cd(II). Int J Miner Process 2016;157:80–8.
[34] Heidarinejad Z, Dehghani MH, Heidari M, Javedan G, Ali I, Sillanpää M. Methods for preparation and activation of activated carbon: a review. Environ Chem Lett 2020;18:393–415.
[35] Qiu ZZ, Zhai YB, Li SH, Liu XM, Liu XP, Wang B, Liu YL, Li CT, Hu YJ. Catalytic co-pyrolysis of sewage sludge and rice husk over biochar catalyst: bio-oil upgrading and catalytic mechanism. Waste Manag 2020;114:225–33.
[36] Saygili H, Guzel F. High surface area mesoporous activated carbon from tomato processing solid waste by zinc chloride activation: process optimization, characterization and dyes adsorption. J Clean Prod 2016;113:995–1004.
[37] Foo KY, Hameed BH. Preparation, characterization and evaluation of adsorptive properties of orange peel based activated carbon via microwave induced K_2CO_3 activation. Bioresour Technol 2012;104:679–86.
[38] Yu MM, Masnadi MS, Grace JR, Bi XT, Lim CJ, Li Y. Co-gasification of biosolids with biomass: thermogravimetric analysis and pilot scale study in a bubbling fluidized bed reactor. Bioresour Technol 2015;175:51–8.
[39] Keown DM, Hayashi J-I, Li C-Z. Drastic changes in biomass char structure and reactivity upon contact with steam. Fuel 2008;87:1127–32.
[40] Reza MS, Afroze S, Kuterbekov K, Kabyshev A, Bekmyrza KZ, Taweekun J, Ja'afar F, Abu Bakar MS, Azad AK, Roy H, Islam MS. Ex situ catalytic pyrolysis of invasive *Pennisetum purpureum* grass with activated carbon for upgrading bio-oil. Sustainability 2023;15.
[41] Zhang S, Wu YF, Wang YM, Zhong M, Wang GJ, Ban YP, Zhao S, Hu HQ, Jin LJ. Facile demineralization of biochar and its catalytic upgrading of bio-oil from fast pyrolysis of bagasse. Fuel 2023;349.
[42] Lu Q, Yang X-c, Dong C-q, Zhang Z-f, Zhang X-m, Zhu X-f. Influence of pyrolysis temperature and time on the cellulose fast pyrolysis products: analytical Py-GC/MS study. J Anal Appl Pyrolysis 2011;92:430–8.
[43] Xin S, Yang H, Chen Y, Yang M, Chen L, Wang X, Chen H. Chemical structure evolution of char during the pyrolysis of cellulose. J Anal Appl Pyrolysis 2015;116:263–71.
[44] Shen DK, Gu S, Bridgwater AV. Study on the pyrolytic behaviour of xylan-based hemicellulose using TG-FTIR and Py-GC-FTIR. J Anal Appl Pyrolysis 2010;88:199–206.